

# Design Optimization of Musculoskeletal Humanoids with Maximization of Redundancy to Compensate for Muscle Rupture

Kento Kawaharazuka<sup>1</sup>, Yasunori Toshimitsu<sup>1</sup>, Manabu Nishiura<sup>1</sup>, Yuya Koga<sup>1</sup>, Yusuke Omura<sup>1</sup>, Yuki Asano<sup>1</sup>, Kei Okada<sup>1</sup>, Koji Kawasaki<sup>2</sup>, and Masayuki Inaba<sup>1</sup>

**Abstract**—Musculoskeletal humanoids have various biomimetic advantages, and the redundant muscle arrangement allowing for variable stiffness control is one of the most important. In this study, we focus on one feature of the redundancy, which enables the humanoid to keep moving even if one of its muscles breaks, an advantage that has not been dealt with in many studies. In order to make the most of this advantage, the design of muscle arrangement is optimized by considering the maximization of minimum available torque that can be exerted when one muscle breaks. This method is applied to the elbow of a musculoskeletal humanoid Musashi with simulations, the design policy is extracted from the optimization results, and its effectiveness is confirmed with the actual robot.

## I. INTRODUCTION

The musculoskeletal humanoid [1]–[4] has various biomimetic advantages such as ball joints without singular points, the flexible spine and fingers, the wide range motion of the scapula, and redundant muscle arrangements allowing for variable stiffness control. Among them, the redundant muscle arrangement is one of its most characteristic structures, with various advantages and disadvantages. So far, using its advantages, variable stiffness control with nonlinear elastic elements [5], [6], balancing and joint coordination with biarticular muscles as well as monoarticular muscles [7], maximization of end-point force and joint angle velocity with redundant muscles [8], etc. have been studied. Also, methods to reduce high muscle tension due to antagonism [9], [10], methods to solve the problem of joint angle speed limited by the slowest muscle [11], etc. have been developed to compensate for its disadvantages.

In this study, we focus on one feature of this redundant muscle arrangement, that is, the advantage of being able to continue to move using the redundant muscles even if one muscle is broken. This feature has not been widely discussed in the past. As related works, a method for calculating muscle tension without using a broken muscle in muscle tension-based control [12] and a method to keep moving even when a muscle breaks through online learning in muscle length-based control [6] have been developed. In humans, the change in the feasible force set when some muscles are paralyzed has been discussed [13]. However, although the

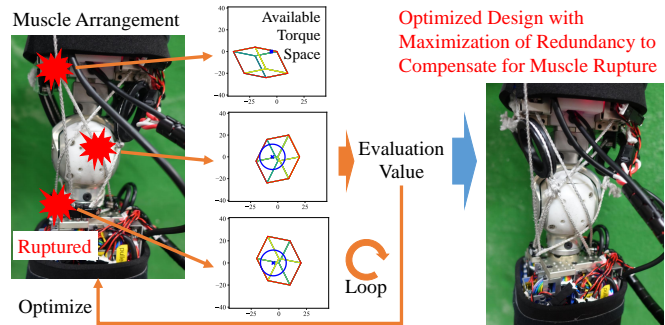


Fig. 1. The concept of this study. By calculating the radius of the hypersphere (blue circle) inscribed in the available torque space (red polygon) when each muscle is broken, an evaluation value is calculated, and the design (muscle Jacobian) is optimized by a genetic algorithm so that the robot can continue to move even when one muscle is broken.

analysis of whether the human body can move as expected when the muscle breaks has been conducted, musculoskeletal humanoids have not yet successfully achieved the performance that allows it to keep moving in all directions even when one muscle is broken.

Therefore, the purpose of this study is a development of body design optimization method for maximizing the redundancy to compensate for muscle rupture. The concept is shown in Fig. 1, which evaluates how the available torque space changes when the muscle breaks and runs an optimization loop. In Section II, we describe the basic structure of musculoskeletal humanoids. In Section III, we describe the calculation of an index for evaluating the redundancy and a design optimization method by maximizing the index. In Section IV, we analyze the optimization results of the 1-DOF (degree of freedom) and 2-DOF joint mechanisms in simulation, and apply them to the musculoskeletal humanoid Musashi [3]. Lastly, the results of the experiments are discussed in Section V and the conclusions are presented in Section VI.

## II. MUSCULOSKELETAL HUMANOIDS

The basic structure of the musculoskeletal humanoid is shown in Fig. 2. The muscles are redundantly arranged around the joint. Muscles that move the joint in the direction of the intended movement are called “agonist muscles” and those that move in the direction that prevents the movement are called “antagonist muscles”. Muscle tension  $f$  and muscle length  $l$  are usually measured. The joint angle cannot usually be measured due to the complexity of the scapula and ball joints, but some robots have joint angle sensors with

<sup>1</sup> The authors are with the Department of Mechano-Informatics, Graduate School of Information Science and Technology, The University of Tokyo, 7-3-1 Hongo, Bunkyo-ku, Tokyo, 113-8656, Japan. [kawaharazuka, toshimitsu, nishiura, koga, oomura, asano, k-okada, inaba@jsk.t.u-tokyo.ac.jp]

<sup>2</sup> The author is associated with TOYOTA MOTOR CORPORATION. koji\_kawasaki@mail.toyota.co.jp

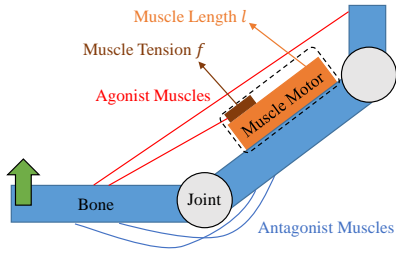


Fig. 2. The basic musculoskeletal structure.

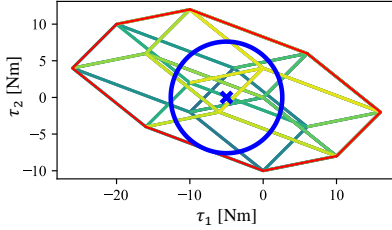


Fig. 3. Hypersphere (blue circle) inscribed in available torque space (red polygon). The line with a gradient from green to yellow is the line where each edge of the available muscle tension space is transformed into the joint torque space.

special mechanisms for learning controls or experimental evaluation.

There are several types of musculoskeletal humanoids. First, there are a few types of actuators, such as those with electric motors and pulleys winding a wire [1], those with pneumatic muscles [14], and those with twisted and coiled polymer (TCP) [15]. Second, there are two types of muscle arrangements: one in which the moment arm of muscles is constant and easy to modelize, and the other in which the moment arm changes like a human being, which is more complicated and difficult to modelize. The musculoskeletal humanoid used in this study uses electric motors and has a complex musculoskeletal structure with variable moment arm like human beings. However, in the case where the moment arm changes, it is difficult to analyze the muscle arrangement numerically. Therefore, we assume that the moment arm is constant to some extent as long as the joint does not move too largely, and analyze the muscle arrangement as if the moment arm is constant.

As for the musculoskeletal humanoid Musashi [3] used in this study, the body is constructed by using muscle modules including motors, gears, pulleys to wind the muscles, muscle tension measurement units, motor drivers, and temperature sensors. The direction in which the muscle exits from the motor module can be arbitrarily changed, and by using three types of muscle relay units, various muscle paths and moment arms can be realized. The muscle wire is made of Dyneema<sup>®</sup>, an abrasion resistant synthetic fiber. The gear ratios of the motors used in this study are all 29:1, and they are backdrivable. In this study, we will consider the problem of determining the maximum value of the moment arm that can be realized, optimizing the muscle Jacobian within that range, and realizing it by arranging the muscle modules and muscle relay units.

### III. DESIGN OPTIMIZATION WITH MAXIMIZATION OF REDUNDANCY TO COMPENSATE FOR MUSCLE RUPTURE

#### A. Calculation of RITS

In this section, we derive an index required to evaluate the redundancy. The basic equations for the musculoskeletal structure are given below,

$$l = h(\theta) \quad (1)$$

$$dl = Gd\theta \quad (2)$$

$$\tau = -G^T f \quad (3)$$

where  $l$  is the muscle length,  $f$  is the muscle tension,  $\theta$  is the joint angle,  $\tau$  is the joint torque,  $h$  is the mapping from  $\theta$  to  $l$ , and  $G$  is the muscle Jacobian. Also,  $\{l, f\}$  are  $M$ -dimensional vectors ( $M$  is the number of muscles) and  $\{\theta, \tau\}$  are  $N$ -dimensional vectors ( $N$  is the number of joints). In the case with the variable moment arm,  $G$  can be expressed as  $G(\theta)$ , and in the case with the constant moment arm,  $G$  is a constant matrix (this study).

The purpose of this section is to obtain the Radius of hypersphere Inscribed in available Torque Space (RITS), which is equivalent to the radius of the blue circle shown in Fig. 3 if the torque space is 2-dimensional. The red line represents the boundary of the available torque space. This is the same idea as the Maximum Isotropic Value (MIV) used in [16], [17], but differs in terms of thinking about joint torque and determining whether the origin exists in the available torque space. Also, basic tendon-driven mechanisms and discussions of feasible force set are detailed in [18]. Since RITS is an index of how much torque can be exerted in all joint directions, the robot can move the body if the value of RITS is greater than zero, even if one muscle is broken. RITS  $r$  can be calculated as follows,

$$\text{maximize} \quad r \quad (4)$$

$$\text{subject to} \quad R \subseteq T \quad (5)$$

$$R := \{\tau \in \mathbb{R}^N \mid |\tau - \tau_g| \leq r\} \quad (6)$$

$$T := \{\tau \in \mathbb{R}^N \mid \exists f \in F, \tau = -G^T f\} \quad (7)$$

$$F := \{f \in \mathbb{R}^M \mid f^{\min} \leq f \leq f^{\max}\} \quad (8)$$

where  $f^{\{min,max\}}$  is the minimum or maximum value of muscle tension, and  $\tau_g$  is the joint torque that must be generated against gravity, friction, or external force. In this study, the  $\tau_g$  is assumed to be constant.

The method to obtain this  $r$  is explained below. First, in Eq. 8, the range of  $f$  can be taken as a  $M$ -dimensional hypercube  $F$ . Then, we can consider the  $F$  to be converted into a  $N$ -dimensional hyperpolyhedron  $T$  by Eq. 3. Here, even if a convex hyperpolyhedron is converted to a hyperpolyhedron by linear transformation, it is still convex. Therefore, we can consider  $r$  to be the radius of the hypersphere inscribed in this  $N$ -dimensional hyperpolyhedron  $T$ . The calculation algorithm can be written as Alg. 1.

First, all the vertices of the hypercube  $F$  are taken out and each of them are projected into the space  $T$  of  $\tau$ . Then, we calculate the convex hull  $C$  of all projected vertices

---

**Algorithm 1** Calculation of RITS  $r$ 

---

```
1: function CalcRITS( $G, \tau_g$ )
2:    $included \leftarrow \text{True}$ 
3:    $p \leftarrow []$ 
4:   for  $v_F$  in all vertices of  $F$  do
5:     push  $-G^T v_F$  to  $p$ 
6:   end for
7:    $C \leftarrow \text{CalcConvexHull}(p)$ 
8:    $c \leftarrow \text{CalcCenter}(C)$ 
9:    $r \leftarrow 1e9$ 
10:  for  $s_C$  in all hyperplanes of  $C$  do
11:     $d_1 \leftarrow \text{CalcDistanceWithSign}(\tau_g, s_C)$ 
12:     $d_2 \leftarrow \text{CalcDistanceWithSign}(c, s_C)$ 
13:    if  $d_1 d_2 < 0$  then
14:       $included \leftarrow \text{False}$ 
15:    end if
16:     $r \leftarrow \min(|d_1|, r)$ 
17:  end for
18:  if not  $included$  then
19:     $r \leftarrow 0$ 
20:  end if
21:  return  $r$ 
22: end function
```

---

(CalcConvexHull). If this  $C$  does not contain the vertex  $\tau_g$ , then the inscribed hypersphere does not exist and we need to remove it. First, we calculate the center point  $c$  that is the average of all vertices in  $C$  that definitely exists in  $C$  (CalcCenter). Then, for all the hyperplanes in  $C$ , we calculate the signed distance  $d_1$  from  $\tau_g$  and that of  $d_2$  from  $c$  (CalcDistanceWithSign). This is equivalent to finding the normal  $a$  of the hyperplane and calculating  $(a^T \tau_g - 1)/\|a\|$  or  $(a^T c - 1)/\|a\|$ . If the product of these two signed distances,  $d_1 d_2$ , is positive, then  $c$  and  $\tau_g$  are on the same side of the hyperplane. If  $\tau_g$  is on the same side of the hyperplane as  $c$  with respect to all the hyperplanes in  $C$ , then  $\tau_g$  exists in  $C$ . If the inscribed hypersphere exists, we calculate the distance  $|d_1|$  from  $\tau_g$  to the hyperplane in  $C$ , and its minimum value is RITS.

### B. Evaluation of Redundancy

For a given design ( $G$ ), we calculate an index representing whether or not the robot with the design continues to move even if one muscle breaks, using RITS. Let  $G_i$  be the  $G$  where the moment arm of the  $i$ -th row of  $G$  becomes zero, i.e. the  $i$ -th muscle is broken. In this study, we use the following  $E$  as the evaluation value,

$$r_0 = \text{CalcRITS}(G, \tau_g) \quad (9)$$

$$r_i = \text{CalcRITS}(G_i, \tau_g) \quad (1 \leq i \leq M) \quad (10)$$

$$E_{value} = \sum_{i=0}^M r_i \quad (11)$$

$$E_{count} = \sum_{i=0}^M \text{Integer}(r_i > 0) \quad (12)$$

$$E = \begin{cases} E_{value} & (E_{count} \geq M_{min} + 1) \\ 0 & (\text{otherwise}) \end{cases} \quad (13)$$

where  $M_{min}$  is the lower limit of the number of muscles that can possibly be broken (only one of these muscles can be broken at a time), and  $\text{Integer}(x)$  is a function that returns 1 if  $x$  is true and 0 if false. That is,  $E_{count} - 1$  is the number of muscles that can possibly be broken, and if  $E_{count} - 1 \geq M_{min}$ , the total RITS value for  $G$  and  $G_i$  for each muscle rupture is  $E$ .

### C. Design Optimization and Detailed Implementation

Based on the obtained  $E$ , we optimize the design ( $G$ ) so that even if one muscle is broken, the remaining muscles can still move the joint. Although there are various ways to do this, we apply a genetic algorithm (GA) in this study. In this section, we explain the experimental setup including concrete values. Using the library [19], we perform crossbreeding with the function `cxBlend` with 50% probability and mutation with the function `mutGaussian` with 20% probability. The individuals are selected by the function `selTournament` and the tournament size is set to 3. The number of individuals is 200 and the number of generations is 50. The minimum and maximum values of muscle Jacobian are set to -0.1 and 0.1 [m], and the values are cropped within the range after each crossing or mutation. For simplicity, we limit the calculation of  $G$  to two decimal places. We set  $F^{min} = 0$  [N] and  $F^{max} = 200$  [N] for the muscle tension. In this study, the experimental results are discussed while changing the number of DOFs  $N$ , the number of muscles  $M$ , the lower limit of the number of muscles that can be broken  $M_{min}$ , and the torque  $\tau_g$  to be generated against gravity, friction, or external force.

TABLE I

THE OPTIMIZED DESIGNS OF 1-DOF TENDON ROBOT. THE VALUES SHOW  $10G^T$ .

	$\tau_g = -5$	$\tau_g = 0$
$M = 3$	$\begin{pmatrix} -1 & 1 & 1 \end{pmatrix}$	No Solution
$M = 4$	$\begin{pmatrix} -1 & 1 & 1 & 1 \end{pmatrix}$	$\begin{pmatrix} -1 & -1 & 1 & 1 \end{pmatrix}$
$M = 5$	$\begin{pmatrix} -1 & -1 & 1 & 1 & 1 \end{pmatrix}$	$\begin{pmatrix} -1 & -1 & 1 & 1 & 1 \end{pmatrix}$
$M = 6$	$\begin{pmatrix} -1 & -1 & -1 & 1 & 1 & 1 \end{pmatrix}$	$\begin{pmatrix} -1 & -1 & -1 & 1 & 1 & 1 \end{pmatrix}$

## IV. EXPERIMENTS

### A. 1-DOF Simulation

Simulation experiments are performed on a robot with  $N = 1$ . The results of the optimization when the parameters are changed to  $M = \{3, 4, 5, 6\}$  and  $\tau_g = \{0, -5\}$  [Nm] are shown in Table I. For ease of viewing, we show  $10G^T$ .  $M_{min}$  is kept constant with  $M_{min} = M$  because the result is the same when  $M_{min}$  is changed except when  $\tau_g = 0$  and  $M = 3$ .

First, in the case of  $M = 3$ , we cannot get a solution. This is because there is only one muscle with positive or negative moment arm, and if it breaks, no torque can be generated in one direction. For  $M \geq 4$ , if  $M$  is even, the best design is one where the numbers of muscles with positive and negative moment arms are the same.

On the other hand, when a constant torque is applied like  $\tau_g = -5$  (e.g., the elbow bent to -90 [deg]), the solution is obtained even for  $M = 3$ . This is because even if the muscle

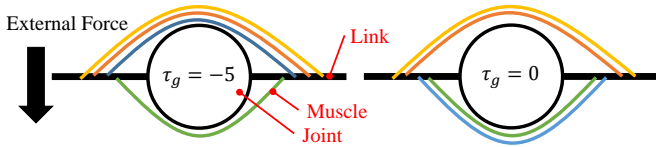


Fig. 4. The optimized design when  $M = 4$  and  $\tau_g = \{-5, 0\}$ .

with negative moment arm breaks, the torque can still be maintained by  $\tau_g$ . In the case of  $M = 4$ , the optimal designs for  $\tau_g = \{-5, 0\}$  are shown in Fig. 4. For the case of  $\tau_g = -5$ , there are three muscles with positive moment arm and one muscle with negative moment arm, while for  $\tau_g = 0$ , there are two muscles with positive moment arm and two muscles with negative moment arm. This means that when  $\tau_g = -5$ , the positive torque is generated ( $\tau_g$  is the joint torque that must be generated against gravity), and the available torque space is greater if the number of muscles with positive moment arm is greater than the number of muscles with negative moment arm.

TABLE II

THE OPTIMIZED DESIGN OF 2-DOF TENDON ROBOT. THE VALUES SHOW  $10G^T$ .

	$\tau_g^T = (-5 \ 0)$	$\tau_g^T = (0 \ 0)$
$M = 4$ ( $M_{min} = 4$ )	$\begin{pmatrix} -0.5 & -0.5 & 1 & 1 \\ -1 & 1 & -0.2 & 0.2 \end{pmatrix}$	No Solution
$M = 4$ ( $M_{min} = 3$ )	$\begin{pmatrix} -1 & 0.7 & 0.8 & 0.8 \\ 0 & 1 & -1 & 1 \end{pmatrix}$	No Solution
$M = 5$ ( $M_{min} = 5$ )	$\begin{pmatrix} -1 & 0.2 & 0.6 & 1 & 1 \\ -0.4 & 1 & 1 & -1 & -0.9 \end{pmatrix}$	$\begin{pmatrix} -1 & -0.8 & 0 & 0.8 & 1 \\ -0.5 & 1 & -1 & 1 & 0.5 \end{pmatrix}$
$M = 5$ ( $M_{min} = 4$ )	$\begin{pmatrix} -1 & -1 & 0.7 & 0.8 & 0.9 \\ 0 & 0.1 & -1 & 1 & -1 \end{pmatrix}$	$\begin{pmatrix} -1 & -1 & 0.5 & 1 & 1 \\ -0.4 & 0.4 & -1 & -1 & 1 \end{pmatrix}$

### B. 2-DOF Simulation

Simulation experiments are performed on a robot with  $N = 2$ . The results of the optimization when the parameters are changed to  $M = \{4, 5\}$ ,  $\tau_g = \{(-5 \ 0)^T, (0 \ 0)^T\}$ , and  $M_{min} = \{M, M-1\}$  are shown in Table II. For ease of viewing, we show  $10G^T$ .

First, in the case of  $\tau_g^T = (0 \ 0)$ , a solution cannot be found for  $M = 4$  and  $M_{min} = \{4, 3\}$ . Therefore, in order to move 2 DOFs and to make the robot continue to move when one of the muscles breaks, at least five muscles are necessary. Then, for  $M = 5$  and  $M_{min} = 5$ , the available torque space and RITS of the optimal design, and their changes when one muscle breaks are shown in Fig. 5. In the optimal design, a large circle is drawn around the origin  $\tau_g$ . It is also shown that the  $\tau_g$  is included in the available torque spaces when muscles are broken one by one, and the joint can be moved in any direction.

Second, in the case of  $\tau_g^T = (-5 \ 0)$ , a solution is obtained even for  $M = 4$ . In contrast to the 1-DOF case, it should be noted that not all moment arms are 1 or -1, but they include values of -0.5 -0.2, and 0.2. The torque space and RITS of the optimal design (A) for  $M = 4$  and  $M_{min} = 4$ , and their changes when the muscles are broken one by one are shown in the upper figure of Fig. 6. The design (A') when absolute value of each moment arm of A is maximized with the same sign, is also shown in the lower figure of Fig. 6. The check

mark at the top right corner of each figure shows whether  $\tau_g$  exists in the available torque space or not. In the design of A, no matter which muscle is broken, the  $\tau_g$  remains in the available torque space and the robot can keep moving. Note that when muscles 1 and 2 break, the RITS is very small, so in order to solve this problem, we can put a restriction on the size of RITS during optimization. However, when the maximum moment arm is distributed evenly to all the joints, as with the design A', when muscles 3 and 4 break, the torque cannot be generated in some directions. In other words, it is necessary to set small values of the moment arm depending on the joint, instead of setting them all at the maximum.

Finally, the results for  $\tau_g^T = (-5 \ 0)$ ,  $M = 4$ , and  $M_{min} = 3$  are shown in Fig. 7. Not limited to these parameters, for  $M_{min} = M - 1$ , the available torque space of the optimized design is likely to be extended in one direction. For the muscles 2 and 3, the RITS does not change when each of the muscles is broken. Also, since  $M_{min} = M - 1$ , for one certain muscle, the robot cannot move when it is broken.

TABLE III

THE HUMAN-MADE DESIGNS OF THE ELBOW OF MUSASHI WITH REFERENCE TO THE OPTIMAL DESIGNS OBTAINED IN SIMULATION. THE VALUES SHOW  $10G^T$ .

original	$\begin{pmatrix} -0.47 & -0.26 & 0.43 & 0.42 \\ -0.17 & 0.20 & -0.15 & 0.24 \end{pmatrix}$
$M = 4, M_{min} = 4$	$\begin{pmatrix} -0.18 & -0.29 & 0.61 & 0.43 \\ -0.10 & 0.20 & -0.043 & 0.036 \end{pmatrix}$
$M = 4, M_{min} = 3$	$\begin{pmatrix} -0.47 & 0.50 & 0.66 & 0.73 \\ 0.047 & -0.19 & -0.30 & 0.18 \end{pmatrix}$

### C. Actual Musculoskeletal Humanoid

For the simulation of  $N = 2$  in Section IV-B, we consider the state of  $M = 4$  and  $\tau_g^T = (-5 \ 0)$ . The left elbow of the musculoskeletal humanoid Musashi [3] has four muscles and two joints, elbow-p and elbow-y (-p and -y means pitch and yaw, respectively). When the elbow is bent about  $-60$  [deg] (the posture is expressed as  $\theta_0$ ), a torque of about  $(-5 \ 0)$  is required for gravity compensation, which is similar to the simulation condition in Section IV-B ( $\tau_g^T = (\tau_{elbow-p} \ \tau_{elbow-y})$ ). Therefore, we modify the muscle arrangement around the elbow with reference to  $G$  obtained from the simulation results to verify the difference in performance on the actual robot Musashi. Note that the muscles of Musashi do not have precise constant moment arms with pulleys, but are wrapped around the ball joints like a human being, so the design is somewhat dependent on the human design and interpretation.

The designed muscle arrangements are shown in Fig. 8. From left to right, they are the original design of Musashi [3] and the designs based on the optimization results of  $M_{min} = 4$  and  $M_{min} = 3$ . Note that the original one is similar to the design in the lower part of Fig. 6.

Since the moment arm cannot be seen from the figure, the relationship between joint angle, muscle tension, and muscle length is learned using the method of [20], and the obtained muscle Jacobian around  $\theta_0$  is shown in Table III. For ease of viewing, we show  $10G^T$ .



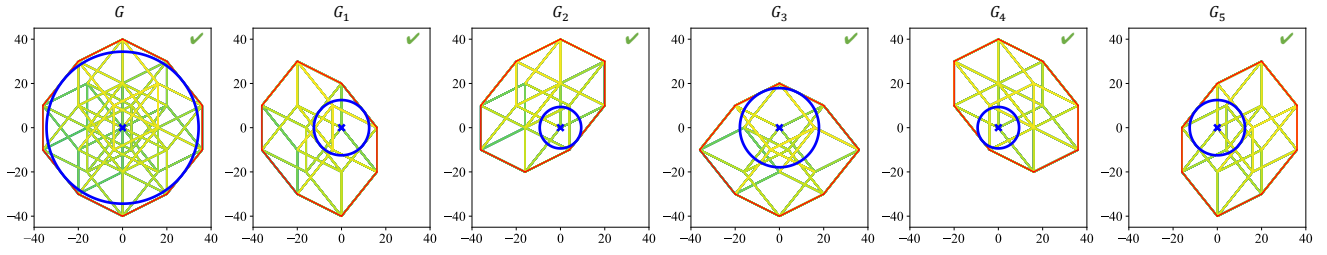


Fig. 5. The available torque space and RITS of the optimized design when  $\tau_g^T = (0 \ 0)$ ,  $M = 5$ , and  $M_{min} = 5$ .

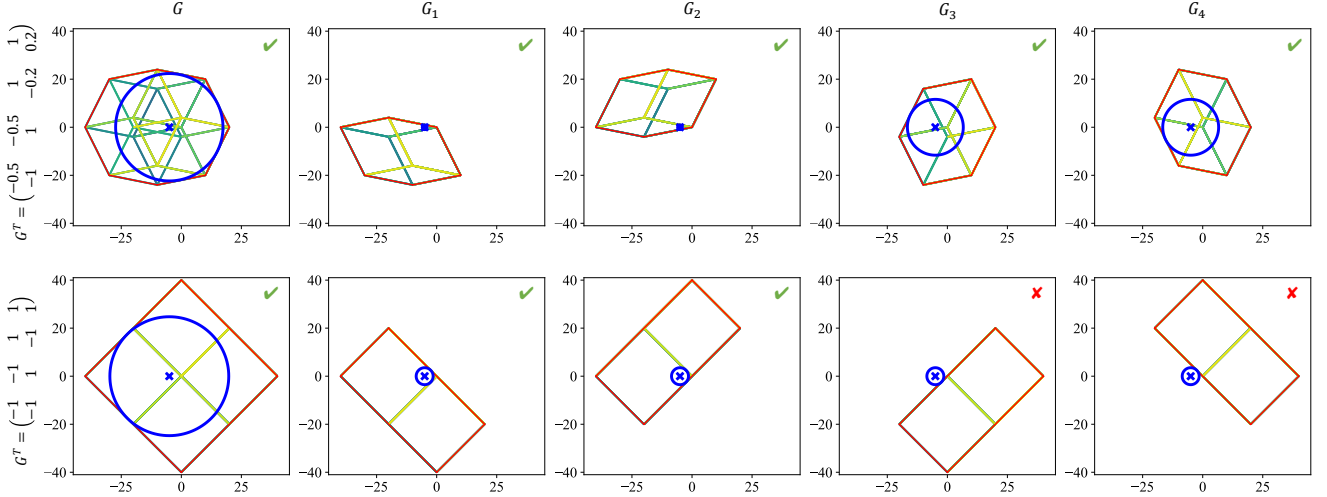


Fig. 6. The available torque space and RITS of the optimized design when  $\tau_g^T = (-5 \ 0)$ ,  $M = 4$ , and  $M_{min} = 4$ , and when absolute value of each moment arm of A is maximized with the same sign.

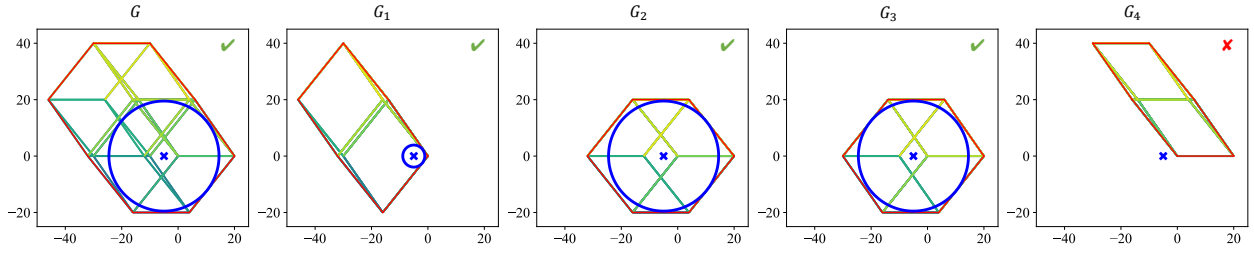


Fig. 7. The available torque space and RITS of the optimized design when  $\tau_g^T = (-5 \ 0)$ ,  $M = 4$ , and  $M_{min} = 3$ .

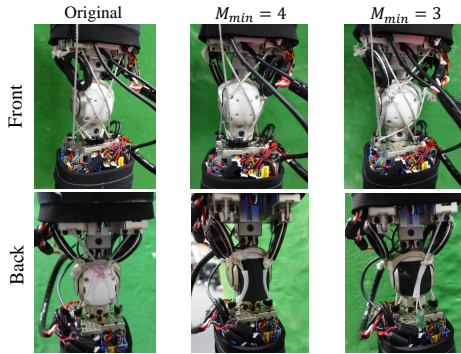


Fig. 8. The original design and optimized designs with  $M_{min} = \{4, 3\}$  of the elbow of Musashi.

While the original design has similar moment arms for each elbow-p and elbow-y, regarding  $M_{min} = 4$ , some moment arms are made small to reduce the interference between muscles. Regarding  $M_{min} = 3$ , three muscles with positive moment arms are used for elbow-p instead of two muscles with positive moment arm and two muscles with

negative moment arm. The available torque space and RITS obtained from the moment arm  $G$  and their changes when muscles are broken one by one are shown in Fig. 9. The available torque space in the direction of elbow-y (y-axis of the figure) is shrunk more than that of Fig. 6 and Fig. 7, because the moment arm for elbow-y is difficult to obtain due to design reasons. The upper part of Fig. 9 and the lower part of Fig. 6, the middle part of Fig. 9 and the upper part of Fig. 6, and the lower part of Fig. 9 and Fig. 7 correspond to each other, and the shape of their available torque space, RITS, and the ability to generate force in any direction are similar to each other.

With these obtained muscle arrangements, six postures of elbow-p and elbow-y around  $\theta_0$  are determined, and the control input is sent to the actual robot using a controller of [20], which is repeated three times. For each of the designs, this experiment is performed for a design with no muscle rupture and for a design with a single muscle rupture (with the motor current set to zero), and the mean and

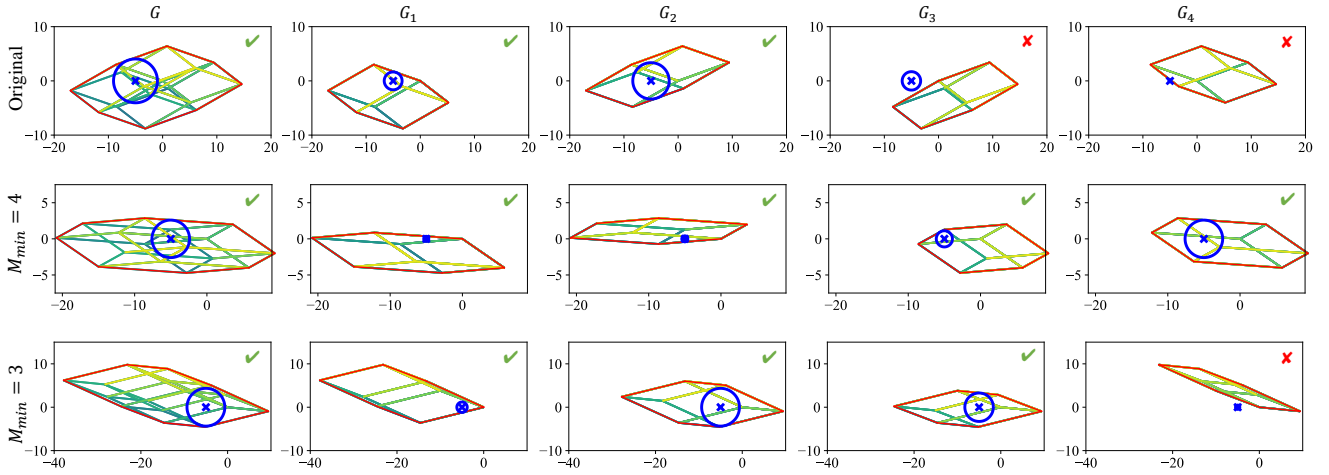


Fig. 9. The available torque space and RITS of the original design of Musashi and the designs based on the optimization results of  $M_{min} = \{4, 3\}$  in Section IV-B.

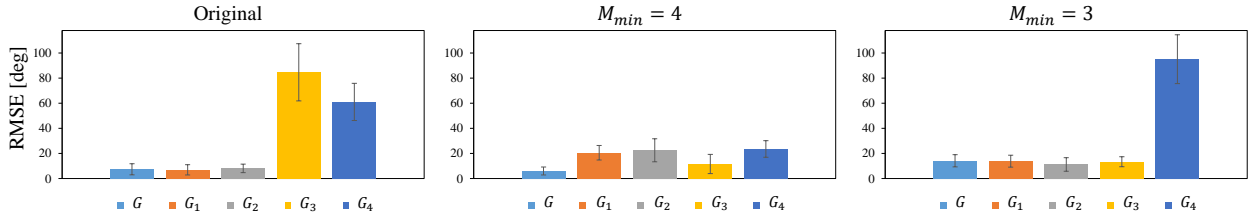


Fig. 10. The average and standard deviation of RMSE between the commanded and measured joint angles when using the original design and the optimized designs with  $M_{min} = \{4, 3\}$ .

variance of the RMSE (Root Mean Squared Error) between the commanded and measured joint angles are calculated. The results are shown in Fig. 10.

In the original design, the RMSE rises so much at the ruptures of the third and fourth muscles that the joints do not move well, and the result is the same as the upper part of Fig. 9. For the optimized design with  $M_{min} = 4$ , the RMSE increases slightly by each muscle rupture, but the body motion is successfully maintained regardless of which muscle is broken. The RMSE regarding the optimized design with  $M_{min} = 3$  increases significantly when the fourth muscle is broken, and the result is the same as the lower part of Fig. 9. Therefore, we found that this method is also effective in the actual robot.

## V. DISCUSSION

We discuss the results obtained from the experiments of this study. First, experiments on the 1-DOF simulation show that the number of muscles with positive and negative moment arms should be as equal as possible in order to maximize the effect of redundancy for the 1-DOF robot with  $\tau_g = 0$ . In this case, the moment arms of all muscles should be the maximum value. If extra force needs to be applied in one direction, as in  $\tau_g = -5$ , by increasing the number of muscles in that direction, the RITS can be large even if one of the muscles is broken.

Next, experiments on the 2-DOF simulation show that in the case with  $\tau_g^T = (0 \ 0)$ , at least five muscles are necessary to be able to move the joint in any direction even if one muscle breaks. This result is consistent with the analysis in [18] that at least  $2N$  muscles are required to move  $N$  DOFs

versatilely. If extra force needs to be applied in one direction, such as in the case of  $\tau_g^T = (-5 \ 0)$ , four muscles may be enough, but the RITS when some muscles are broken may be very small. Also, unlike the case of the 1-DOF robot, if the absolute value of each moment arm is set to the maximum, the joint will not be able to make use of the redundancy because the balance of muscle tensions will not be maintained when one muscle is broken. Therefore, in order to take advantage of the redundancy, it is important to reduce moment arms of some muscles to half or less. Also, if we relax the constraint of  $M_{min}$  like  $M_{min} = M - 1$ , we can derive a design in which one of the muscles plays an important role and RITS can be kept large when the rest of the muscles is broken. Since only the important muscle is required to be protected, we can consider taking advantage of the redundancy by actively using such a design.

Finally, from the actual robot experiments of Musashi, it is shown that the same performance can be obtained for the actual robot by imitating the optimal design obtained in simulations. Although the difference between the commanded and the realized joint angles may be larger when the RITS is small due to the influence of friction, which is difficult to modelize on the actual robot, the characteristics of the actual robot are almost the same with the simulation results. Therefore, it is expected that the muscle arrangement can be modified based on the simulation results to create a robust body that can continue to move even if one muscle breaks.

The limitations of this study are described below. First, although this study can be applied to the general system with more than two degrees of freedom, the computational

complexity of  $E$  depends on calculation of all the vertices of the hypercube  $F$  in the RITS calculation  $O(2^M)$ , and therefore, it explodes exponentially with the number of muscles. Since the number of muscles should be increased as the number of joints increases, the limit is currently about  $N = 3$  and  $M = 7$ , and the speed of the algorithm should be increased. Using the conversion between span-form and face-form [21] is one of its solutions. Second, the optimization is performed based on the approximation of constant moment arm, and it is applied to the design of human-like joints where the moment arm is not constant. Therefore, we kept  $N = 2$  in this study because the more  $N$  is increased, the more the design depends on the human interpretation. In the future, it is necessary to make a method generally applicable to the system with variable moment arms. We also would like to complete a series of processes as in [22], which detects physical changes such as a muscle break, relearns self-models, and adapts to the real world.

## VI. CONCLUSION

In this study, we proposed a body design analysis and optimization method to take advantage of the redundant muscle arrangement in musculoskeletal humanoids, which allows the body to continue to move even if one muscle breaks. We described the method of maximizing the radius of the hypersphere inscribed in the hyperpolyhedron of the available joint torque space (RITS) when the muscles are broken one by one. The simulation experiments show that instead of having all moment arms arranged in the same way, it is possible to make some moment arms smaller so that the robot can continue to move even if one muscle is broken. Depending on the evaluation function of the optimization, it is also possible to create a biased design where the load is concentrated on one muscle and the robot can move even if any of the other muscles break. The application of this study to the actual musculoskeletal humanoid generated the same results as in the simulations, which confirmed the effectiveness of this study.

In future works, we would like to extend these results to the whole body design to make the robot more robust.

## REFERENCES

- [1] Y. Nakanishi, S. Ohta, T. Shirai, Y. Asano, T. Kozuki, Y. Kakehashi, H. Mizoguchi, T. Kurotobi, Y. Motegi, K. Sasabuchi, J. Urata, K. Okada, I. Mizuuchi, and M. Inaba, "Design Approach of Biologically-Inspired Musculoskeletal Humanoids," *International Journal of Advanced Robotic Systems*, vol. 10, no. 4, pp. 216–228, 2013.
- [2] S. Wittmeier, C. Alessandro, N. Bascarevic, K. Dalamagkidis, D. Devereux, A. Diamond, M. Jäntschi, K. Jovanovic, R. Knight, H. G. Marques, P. Milosavljevic, B. Mitra, B. Svetozarevic, V. Potkonjak, R. Pfeifer, A. Knoll, and O. Holland, "Toward Anthropomorphic Robotics: Development, Simulation, and Control of a Musculoskeletal Torso," *Artificial Life*, vol. 19, no. 1, pp. 171–193, 2013.
- [3] K. Kawaharazuka, S. Makino, K. Tsuzuki, M. Onitsuka, Y. Nagamatsu, K. Shinjo, T. Makabe, Y. Asano, K. Okada, K. Kawasaki, and M. Inaba, "Component Modularized Design of Musculoskeletal Humanoid Platform Musashi to Investigate Learning Control Systems," in *Proceedings of the 2019 IEEE/RSJ International Conference on Intelligent Robots and Systems*, 2019, pp. 7294–7301.
- [4] M. Jäntschi, S. Wittmeier, K. Dalamagkidis, A. Panos, F. Volkart, and A. Knoll, "Anthrob - A Printed Anthropomorphic Robot," in *Proceedings of the 2013 IEEE-RAS International Conference on Humanoid Robots*, 2013, pp. 342–347.
- [5] H. Kobayashi, K. Hyodo, and D. Ogane, "On Tendon-Driven Robotic Mechanisms with Redundant Tendons," *The International Journal of Robotics Research*, vol. 17, no. 5, pp. 561–571, 1998.
- [6] K. Kawaharazuka, K. Tsuzuki, S. Makino, M. Onitsuka, Y. Asano, K. Okada, K. Kawasaki, and M. Inaba, "Long-time Self-body Image Acquisition and its Application to the Control of Musculoskeletal Structures," *IEEE Robotics and Automation Letters*, vol. 4, no. 3, pp. 2965–2972, 2019.
- [7] M. A. Sharbafi, C. Rode, S. Kurowski, D. Scholz, R. Möckel, K. Radkhah, G. Zhao, A. M. Rashty, O. V. Stryk, and A. Seyfarth, "A new biarticular actuator design facilitates control of leg function in BioBiped3," *Bioinspiration & Biomimetics*, vol. 11, no. 4, p. 046003, 2016.
- [8] A. Marjaninejad and F. J. Valero-Cuevas, *Should Anthropomorphic Systems be "Redundant"?* Springer, 2019, pp. 7–34.
- [9] K. Kawaharazuka, M. Kawamura, S. Makino, Y. Asano, K. Okada, and M. Inaba, "Antagonist Inhibition Control in Redundant Tendon-driven Structures Based on Human Reciprocal Innervation for Wide Range Limb Motion of Musculoskeletal Humanoids," *IEEE Robotics and Automation Letters*, vol. 2, no. 4, pp. 2119–2126, 2017.
- [10] Y. Koga, K. Kawaharazuka, M. Onitsuka, T. Makabe, K. Tsuzuki, Y. Omura, Y. Asano, K. Okada, and M. Inaba, "Modification of Muscle Antagonistic Relations and Hand Trajectory on the Dynamic Motion of Musculoskeletal Humanoid," in *Proceedings of the 2019 IEEE-RAS International Conference on Humanoid Robots*, 2019, pp. 632–637.
- [11] K. Kawaharazuka, Y. Koga, K. Tsuzuki, M. Onitsuka, Y. Asano, K. Okada, K. Kawasaki, and M. Inaba, "Exceeding the Maximum Speed Limit of the Joint Angle for the Redundant Tendon-driven Structures of Musculoskeletal Humanoids," in *Proceedings of the 2020 IEEE/RSJ International Conference on Intelligent Robots and Systems*, 2020, pp. 3585–3590.
- [12] M. Kawamura, S. Ookubo, Y. Asano, T. Kozuki, K. Okada, and M. Inaba, "A Joint-Space Controller Based on Redundant Muscle Tension for Multiple DOF Joints in Musculoskeletal Humanoids," in *Proceedings of the 2016 IEEE-RAS International Conference on Humanoid Robots*, 2016, pp. 814–819.
- [13] L. Kuxhaus, S. S. Roach, and F. J. Valero-Cuevas, "Quantifying deficits in the 3D force capabilities of a digit caused by selective paralysis: application to the thumb with simulated low ulnar nerve palsy," *Journal of Biomechanics*, vol. 38, no. 4, pp. 725–736, 2005.
- [14] R. Niyama and Y. Kuniyoshi, "Design principle based on maximum output force profile for a musculoskeletal robot," *Industrial Robot: An International Journal*, vol. 37, no. 3, pp. 1–6, 2010.
- [15] Y. Almubarak and Y. Tadesse, "Twisted and coiled polymer (TCP) muscles embedded in silicone elastomer for use in soft robot," *International Journal of Intelligent Robotics and Applications*, vol. 1, no. 3, pp. 352–368, 2017.
- [16] R. Finotello, T. Grasso, G. Rossi, and A. Terribile, "Computation of kinetostatic performances of robot manipulators with polytopes," in *Proceedings of the 1998 IEEE International Conference on Robotics and Automation*, 1998, pp. 3241–3246.
- [17] J. M. Inouye and F. J. Valero-Cuevas, "Anthropomorphic tendon-driven robotic hands can exceed human grasping capabilities following optimization," *The International Journal of Robotics Research*, vol. 33, no. 5, pp. 694–705, 2014.
- [18] F. J. Valero-Cuevas, *Fundamentals of Neuromechanics*, ser. Biosystems & Biorobotics. Springer-Verlag, London, 2015, vol. 8.
- [19] F. Fortin, F. D. Rainville, M. Gardner, M. Parizeau, and C. Gagné, "DEAP: Evolutionary Algorithms Made Easy," *Journal of Machine Learning Research*, vol. 13, pp. 2171–2175, 2012.
- [20] K. Kawaharazuka, K. Tsuzuki, M. Onitsuka, Y. Asano, K. Okada, K. Kawasaki, and M. Inaba, "Musculoskeletal AutoEncoder: A Unified Online Acquisition Method of Intersensory Networks for State Estimation, Control, and Simulation of Musculoskeletal Humanoids," *IEEE Robotics and Automation Letters*, vol. 5, no. 2, pp. 2411–2418, 2020.
- [21] K. Fukuda and A. Prodon, "Double description method revisited," in *Combinatorics and Computer Science*, 1996, pp. 91–111.
- [22] R. Kwiatkowski and H. Lipson, "Task-agnostic self-modeling machines," *Science Robotics*, vol. 4, no. 26, 2019.